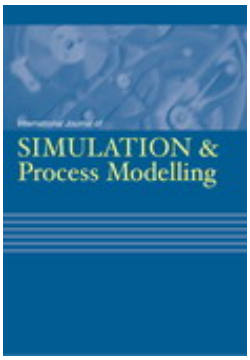

International Journal of Simulation and Process Modelling

ISSN online: 1740-2131 - ISSN print: 1740-2123
https://www.inderscience.com/ijspm

Numerical study of sago pith waste drying process in a fluidised bed dryer

Angnes Ngieng Tze Tiong, Eunice Ke Xin Lou

DOI: 10.1504/IJSPM.2023.10057078

Article History:

Received:	24 October 2022
Last revised:	21 March 2023
Accepted:	21 March 2023
Published online:	26 October 2023

Numerical study of sago pith waste drying process in a fluidised bed dryer

Angnes Ngieng Tze Tiong* and Eunice Ke Xin Lou

Department of Chemical and Energy Engineering,
Curtin University Malaysia,
CDT 250, 98009 Miri Sarawak, Malaysia
Email: angnesnt@curtin.edu.my
Email: 700023756@student.curtin.edu.my
*Corresponding author

Abstract: Research on the drying of sago pith waste (SPW) using a fluidised bed dryer (FBD) is relatively scarce. Therefore, it was the aim of this study to scrutinise the drying of SPW in the FBD with varying diameter and height through computational fluid dynamic modelling. The simulations were conducted by using the multiphase Eulerian-Eulerian approach. The effects of bed dimensions, air velocity, and air temperature on the drying performance of SPW were investigated. Better drying of SPW is attained in FBD with a larger height and smaller diameter. Besides, the drying performance is better when the air temperature increases from 50°C to 100°C. Higher inlet velocities of 3 m/s to 4 m/s are not recommended. The recommended diameter and height for FBD are 180 mm and 190 mm, respectively. The optimum operating conditions to achieve the desired final moisture content are 1–2 m/s of air inlet velocities and an inlet temperature of 50°C.

Keywords: computational fluid dynamics; CFD; drying; fluidised bed dryer; FBD; sago pith waste; SPW.

Reference to this paper should be made as follows: Tiong, A.N.T. and Lou, E.K.X. (2023) 'Numerical study of sago pith waste drying process in a fluidised bed dryer', *Int. J. Simulation and Process Modelling*, Vol. 20, No. 1, pp.31–38.

Biographical notes: Angnes Ngieng Tze Tiong received her PhD and Bachelor's in Chemical Engineering from Curtin University Malaysia. She is currently a Lecturer at the Department of Chemical and Energy Engineering, Curtin University Malaysia. Her research interests are in the areas related to process heat transfer, computational fluid dynamics, process simulation and process optimisation.

Eunice Ke Xin Lou has received her Bachelor's in Chemical Engineering from Curtin University Malaysia.

1 Introduction

In recent years, sago palms have been gaining much importance as starch crops for sustainable agriculture. 'Sago' is a Javanese term that means starch-containing palm pith. It is known as '*Metroxylon sagu*' scientifically. Sago palms are considered 'the 21st century's starch crop' by many scientists across the world and are said to be environmentally friendly, and economically acceptable, as well as help to improve the socially stable agroforestry system (Zhu, 2019). They are often known to have great abilities to prosper in a moist environment and even under unfavourable soil conditions such as peat soils of low nutrient status. Hence, they are frequently found along riverbanks, water holes, and swampy areas (Amin et al., 2019). Aside from that, they also have great tolerances in tropical acidic marshy grounds that are hardly utilised as farmlands. Sago palms are unaffected by drought, fires, floods, and intense winds due to their large fibrous root system that helps to trap silt loads and extract pollutants, heavy metals, and spoiled contaminants (Ehara et al., 2018).

Sago palms are an endemic species in Southeast Asia, especially in Papua New Guinea, Indonesia, Malaysia, and Philippines. Currently, Papua New Guinea, Indonesia, and Malaysia are the three leading producers of sago in which sago palms are harvested to obtain sago starch. When comparing sago palms with other common starch crops such as rice, corn, or cassava, it has a much higher production capacity that can reach up to 25 tons/ha per year which is estimated based on a stand of 150 palms per hectare annually and 175 kg of starch per palm. This is the highest possibly reached production capacity among the starchy crops of the world (Singhal et al., 2008). Following Indonesia and Papua New Guinea, Malaysia ranks third in the world for the production of sago starch, whereby it is estimated that 94.6% of the world's sago starch is produced by these three countries in total. Even though Indonesia and Papua New Guinea have higher production of sago starch

than Malaysia, the sago industry in Malaysia is somehow considered as well established, having more than 90.0% of sago-planting areas available in the state of Sarawak, especially in the Mukah division in Malaysia. Meanwhile, the sago industry has been listed as one of the most important production industries especially benefiting the country's export revenue by which about 25,000 to 40,000 tons of sago products are exported to Peninsular Malaysia, Taiwan, Japan, and Singapore annually (Amin et al., 2019).

Starch in the sago palms trunk will normally accumulate until the flowering stage when it reaches the maximum starch content. The starch present in the sago palm pith is intended to be separated from cellulosic materials through various stages of processing procedures to extract starch that has excellent quality in high quantity. The sago starch extraction process can normally be carried out either through the traditional or modern method, with both methods having similar principles but with different scales of operations instead. While extracting sago starch, the bark-like layer of the palm must be removed first. After that, the palm will be undergoing a rasping process in favour of shattering the pith and loosening the starch particles within the fibre, so that it will become soft. From there, the starch is separated away from the fibre possibly either by spraying it with water, trampling using feet, or kneading with hand. After the starch has been removed, it will then go through a series of centrifugal sieves for the removal of the coarse fibres remaining. It is then extracted using cyclone-type of separators and dried with a rotary drum dryer and further dried utilising hot air (Amin et al., 2019).

In Malaysia, the state of Sarawak is consistently producing massive quantities of agricultural residues from sago starch processing industries, making them always readily available. Approximately 7 tons of sago pith waste (SPW) is produced daily from a single sago starch processing mill (Awg-Adeni et al., 2009). The SPW is a fibrous waste formed after the starch extraction from the rasped sago palm pith, with 82% moisture content and 62% starch content (dry weight basis). It is also known as sago *hampas* (Lai et al., 2013). This agricultural residue tends to be discharged into streams nearby together with the wastewater produced. Due to that, serious environmental issues and pollution often occur. Thus, taking advantage of its natural properties, they are desired to be transformed into value-added products. It is not only able to reduce the pollution issues caused but an economic solution for waste management system at sago processing mills will also be contributed by utilising those sago residues.

The SPW has a high potential to be used as sustainable feedstock considering its availability and especially its significant content of starchy-lignocellulosic compounds. For example, it is recognised as a potential substrate for solid substrate fermentation either by enzyme or acid hydrolysis or by fungal bioconversion (Awg-Adeni et al., 2009). Besides, the SPW can be used as animal feed, the substrate for confectioners syrup production, compost for mushroom culture, etc. (Phang et al., 2000). It can also be transformed into thermoplastic starch composites without any addition of a binder (Lai et al., 2013).

Before the SPW can be converted into marketable value-added products, its moisture content needs to be reduced through the drying process. The drying methods which have been used for the conversion of SPW are for example microwave drying, solar drying, fluidised bed dryer (FBD), as well as heat pump. The FBD is considered the most widely used approach among all the other possible drying methods mentioned as it offers more advantages. The FBD is often recognised for its high mass transfer rates and drying rates due to excellent gas-solid contact, high thermal energy efficiency, good solids mixing, shorter drying time, easy operation and maintenance, and relatively low capital cost (Rosli et al., 2020, 2018; Othman et al., 2020). Moreover, the temperature in FBD can be monitored well, thus making the drying of heat-sensitive products effective (Alaathar et al., 2013).

Drying monitoring using computational fluid dynamics (CFD) is more beneficial than experimental work, especially when the information on optimum operating conditions required for the drying process is limited (Rosli et al., 2018). The CFD approach provides an understanding of flow, heat, and mass transfer which is too complex to be comprehended using experiments. Moreover, the CFD technique is also not as time-consuming and expensive as the experimental approach (Li et al., 2022; Liu, 2022). For these reasons, numerical modelling using the CFD model is usually implemented to analyse the drying performances of SPW taking place in FBD as the CFD modelling can help to improve the scientific insights on drying and thus optimise the process (Othman et al., 2020; Mortier et al., 2011).

To date, the study of SPW drying using FBD is relatively scarce. More drying studies using FBD are done for other products like carrots, corn, pharmaceutical wet granules, etc. (Tayyeb et al., 2013; Azmir et al., 2018; Suherman et al., 2018; Nabizadeh et al., 2020; Aziz et al., 2022). The investigations of the SPW drying process in the FBD were mainly focusing on varying the operating conditions in the FBD for better drying performances (Nasir et al., 2021; Othman et al., 2020; Rosli et al., 2018). For example, a recent numerical investigation was carried out by Rosli et al. (2018), focusing on finding a particle size and a drying air velocity for the optimal drying process of SPW. Othman et al. (2020) concluded that a greater drying rate could be achieved with a higher inlet temperature and air velocity. Besides, Nasir et al. (2021) determined the fluidisation profile and the moisture content of the SPW drying process. However, the study on how the sizes of an FBD affect the drying performances of SPW is lacking. The optimal operating condition (air inlet temperature and velocity) when the size of FBD is varied is not known clearly. Therefore, this research aims to fulfil these research gaps. Given the essential role played by these parameters (FBD size, inlet air temperature and air velocity), the outcomes of this study aid to provide a better understanding of their contribution to the drying process of SPW in the FBD. This project also hopes to emphasise the potential of

reusing the waste from sago processing industries for better sustainability, which is related to sustainable development goal no. 12- responsible consumption and production.

Figure 1 Geometry of FBD created for simulation (see online version for colours)

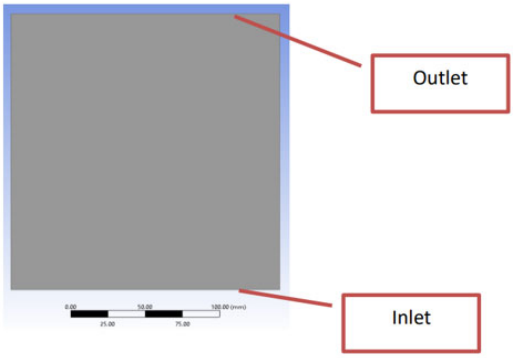

Table 1 Dimensions of FBD considered in this study

Geometry	*Height, H (mm)*	*Diameter, D (mm)*
1	220	140
2	220	160
3	220	180
4	220	200
5	220	210
6	190	180
7	200	180
8	220	180
9	240	180
10	260	180

2 Methodology

2.1 Geometry creation

The FBD is simulated in a 2-dimensional model as shown in Figure 1, the inlet of the FBD was at the bottom while the outlet of the FBD was at the top. The two sides would be the domain walls for the FBD. The height and the diameter of the FBD were varied for this study and the dimensions considered are listed in Table 1.

2.2 Governing equation

The Eulerian-Eulerian multiphase model was selected to be employed in this research study as it is extensively used for modelling a gas-solid flow (Nasir et al., 2021; Rosli et al., 2018). The Eulerian multiphase model designated was made up of two Eulerian phases consisting of air as the gas phase and the SPW particles as the solid phase. The conservation of mass, momentum, and energy governing equations shown in equations (1), (2), and (4), respectively, were adopted to solve the drying of SPW in an FBD numerically (ANSYS, 2013).

$$\frac{\partial}{\partial t}(\alpha_q \rho_q) + \nabla \cdot (\alpha_q \rho_q \vec{v}_q) = \sum_{p=1}^{n} (\dot{m}_{pq} - \dot{m}_{qp}) + S_q \tag{1}$$

$$\begin{aligned} &\frac{\partial}{\partial t}(\alpha_q \rho_q \vec{v}_q) + \nabla \cdot (\alpha_q \rho_q \vec{v}_q \vec{v}_q) = \\ &\quad -\alpha q \nabla p + \nabla \cdot \overline{\overline{\tau}}_q + \alpha_q \rho_q \vec{g} \\ &\quad + \sum_{p=1}^{N} \left(\vec{R}_{pq} + \dot{m}_{pq} \vec{v}_{pq} - \dot{m}_{qp} \vec{v}_{qp} \right) \\ &\quad + \left(\vec{F}_q + \vec{F}_{lift,q} + \vec{F}_{vm,q} + \vec{F}_{td,q} \right) \end{aligned} \tag{2}$$

$$\overline{\overline{\tau}}_q = \alpha_q \mu_q + \left(\nabla \vec{v}_q + \nabla \vec{v}_q{}^T \right) + \alpha_q \left(\lambda_q - \frac{3}{2} \mu_q \right) \nabla \cdot \vec{v}_q \overline{\overline{I}} \tag{3}$$

$$\begin{aligned} &\frac{\partial}{\partial t}(\alpha_q \rho_q h_q) + \nabla \cdot (\alpha_q \rho_q \vec{v}_q h_q) = \alpha_q \frac{\partial_{pq}}{\partial t} + \overline{\overline{\tau}}_q : \nabla \vec{v}_q \\ &\quad -\nabla \cdot \vec{q}_q + Sq + \sum\nolimits_{p=1}^{n} (Q_{pq} + \dot{m}_{pq} h_{pq} - \dot{m}_{qp} h_{qp}) \end{aligned} \tag{4}$$

where α_q is the volume fraction of phase q, ρ_q is the density of q phase, $\vec{v}_q$ is the velocity for phase q, $\dot{m}_{pq}$ is the mass transfer from p^{th} to q^{th} phase, $\dot{m}_{qp}$ is the mass transfer from q^{th} to p^{th} phase, p is the pressure shared by all phases, $\overline{\overline{\tau}}_q$ is the q^{th} phase stress-strain tensor, g is the gravitational acceleration, $\vec{R}_{pq}$ is the interaction force between phases, $\vec{v}_{pq}$ and $\vec{v}_{qp}$ are interphase velocities, $\vec{F}_q$ is the external body force, $\vec{F}_{lift,q}$ is the lift force, $\vec{F}_{wl,\,q}$ is the wall lubrication force, $\vec{F}_{vm,q}$ is the virtual mass force, $\vec{F}_{td,q}$ is the turbulent dispersion force, μ_q and λ_q are the shear and bulk viscosity of phase q, S_q is the source of enthalpy, h_q is the specific enthalpy of q^{th} phase, $\vec{q}_q$ is the heat flux, Q_{pq} is the intensity of heat exchange between the p^{th} and q^{th} phases, h_{pq} and h_{qp} are the interphase enthalpies, and $\overline{\overline{I}}$ is the unit tensor.

The turbulence of the flow was modelled using the standard k-epsilon model, which is shown in equations (5) and (6) (ANSYS, 2013).

$$\begin{aligned} &\frac{\partial}{\partial t}(\rho k) + \frac{\partial}{\partial_{xi}}(\rho k u_i) = \frac{\partial}{\partial x_j}\left[\left(\mu + \frac{\mu_t}{\sigma_k} \right) \frac{\partial_k}{\partial_{xj}} \right] \\ &\quad + G_k + G_b - \rho\varepsilon - Y_M + Sk \end{aligned} \tag{5}$$

$$\begin{aligned} &\frac{\partial}{\partial_t} + \frac{\partial}{\partial_{xi}}(\rho \varepsilon u_i) = \frac{\partial}{\partial_{xj}}\left[\left(\mu + \frac{\mu_t}{\sigma_\varepsilon} \right) \right] C_{1\varepsilon} \frac{\partial}{k}(G_k + C_{3\varepsilon} G_b) \\ &\quad - C2\varepsilon\rho \frac{\varepsilon^2}{k} + S\varepsilon \end{aligned} \tag{6}$$

where k is the turbulence kinetic energy, ε is the turbulence dissipation rate, μ is the viscosity, μ_t is the turbulent viscosity, G_k is the generation of turbulence kinetic energy due to mean velocity gradients, G_b is the generation of turbulence kinetic energy due to buoyancy, Y_M is the contribution of the fluctuating dilatation in compressible turbulence to the overall rate, ($C_{1\varepsilon}$, $C_{\varepsilon 2}$, $C_{\varepsilon 3}$) are constants,

and (S_k and S_ε) are the user-defined source terms. σ_k and σ_ε are the turbulent Prandtl numbers for k and ε, respectively. The values for the constants are: $C_{1\varepsilon} = 1.44$, $C_{2\varepsilon} = 1.92$, k = 1.0, and = 1.3 (ANSYS, 2013).

Apart from that, the moisture content ratio was estimated using the two-term exponential model, which is defined in equation (7) (Nasir et al., 2021; Rosli et al., 2018).

$$MR = a\exp(-kt) + (1-a)\exp(-kat) \tag{7}$$

$$k = (4.882\times10^{-4}T) + (1.506\times10^{-3}v) - (2.23\times10^{-3}) \tag{8}$$

where MR is the moisture ratio, k is the drying constant, T is the air temperature, v is the air velocity, t is the drying time, and a is the constant with a value of 2.0888.

2.3 Boundary conditions

The simulation in this research was conducted in a transient condition. Some assumptions were made to solve the formulated governing equations. These assumptions were listed as follows:

1 Uniform sago particle size of 2,000 m. Fluidisation can happen easily with this particle size (Nasir et al., 2021; Rosli et al., 2018).

2 Negligible particle size reduction during the drying process.

3 The initial moisture content of the SPW was at 40%.

4 The SPW did not accumulate at a moisture content of 40%.

5 No slip condition on the walls of FBD.

6 No chemical reaction during the drying process.

7 Uniform inlet air velocity.

8 The thermal properties of SPW were similar to those of cassava (Nasir et al., 2021; Rosli et al., 2018; Lamidi et al., 2019; Othman et al., 2020).

9 The SPW was loaded in the FBD at the beginning of the simulation.

10 The FBD was well-mixed.

The pressure-based solver was used for this study. A gravitational setup of 9.81 m/s^2 is activated. Air served as the primary phase while the SPW is the secondary phase. A standard wall function was adopted for the near-wall treatment. The air velocity, v considered ranged from 1 m/s to 4 m/s. To fix the SPW in the bed within the initial bed height, its inlet velocity was set to 0 m/s. Uniform air temperature, T was utilised with its value varied from 50°C to 100°C. The pressure outlet was employed to minimise the reversed flow during the computation. The initial solid volume fraction of SPW was 0.45 while the initial bed height was 0.023 m.

2.4 Numerical solution procedure

For the pressure velocity coupling in the multiphase model, the phased coupled semi-implicit method for pressure-linked equations (SIMPLE) was implemented. First-order implicit was chosen for the transient formulation (Rosli et al., 2018). Besides, first-order upwind was selected for the spatial discretisation of volume fraction, turbulent kinetic energy, turbulent dissipation rate, and energy. Least squares cell-based and PRESTO was utilised for the gradient and pressure spatial discretisation, respectively. For the spatial discretisation of momentum, second-order upwind was used. The simulations were performed using 1,000 time steps with a time step size of 0.01 s.

Figure 2 Grid independence study for FBD with a diameter of 140 mm and height of 220 mm (see online version for colours)

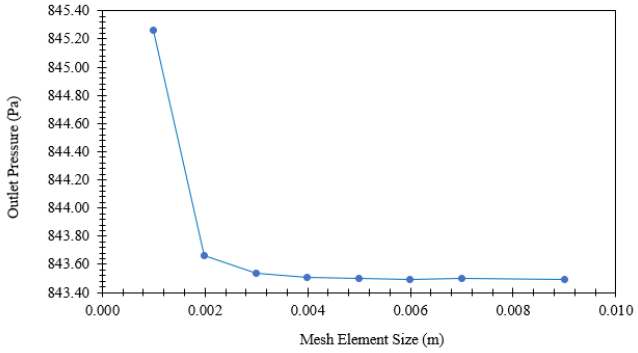

3 Grid independency

To obtain accurate and precise results for simulation, a mesh independency test was performed. Mesh element size was varied to change the mesh element and node. One of the results for the mesh independency test is depicted in Figure 2. It can be observed that the outlet total pressure starts to become constant when the mesh element size varies from 0.003 m onwards. There is less than a 5% differential in the outlet total pressure from 0.003 m onwards. Therefore, a 0.003 m mesh element size was chosen for the FBD with a diameter and height of 140 mm and 220 mm, respectively. Similar mesh independency tests were completed for all the other geometries studied.

4 Validation

After conducting the grid independency study, it was then followed by the validation study. The results from Rosli et al. (2018) were used for validation purposes, with the diameter and height of the FBD of 180 mm and 220 mm, respectively. The inlet air velocity was increased from 0.6 m/s to 2.2 m/s, following those of Rosli et al. (2018). Besides, the initial solid volume fraction of SPW of 0.45 and the initial bed height of 0.023 m before the drying were employed. The bed height of the SPW fluidised is plotted in Figure 3. It can be noticed that the results of this present

study agree well with the data from Rosli et al. (2018), with a maximum deviation of merely 4.7%. Therefore, the simulation setup and the numerical solution procedure of this present simulation study are valid and reasonable.

Figure 3 Comparison of results between the present study and Rosli et al. (2018)

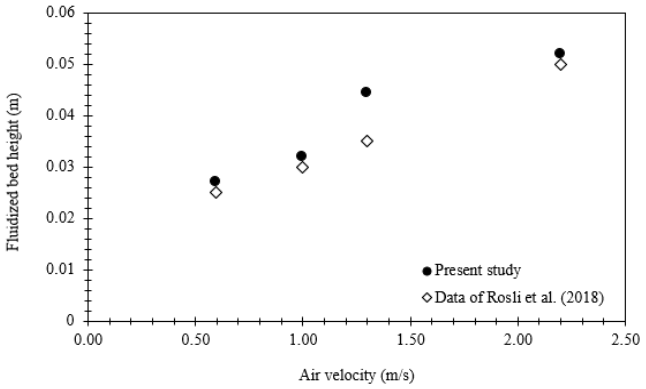

5 Results and discussion

5.1 Effect of dimension of FBD on the drying of SPW

The first part of this study investigates the effect of the diameter of FBD on the drying performance of the SPW. After undergoing fluidisation in the FBD, the moisture content ratio of SPW has decreased from its initial value of 0.4. The final moisture ratio result is illustrated in Figure 4. It was observed that the final moisture content ratio of the SPW increases with the increasing diameter of FBD. The final moisture content ratio is increased by 66.4% when the bed diameter is increased from 140 mm to 210 mm. The results in Figure 4 indicate that more effective fluidisation is achieved in the FBD with a smaller diameter. For effective fluidisation, a better mixing between the SPW and the air is attained, leading to a superior drying performance. Hence, the final moisture content ratio of the SPW is lower. This finding agrees well with that obtained by Sarker et al. (2012) that a column with a smaller diameter promotes better drying performance. However, some researchers (Rao et al., 2010; Basrawi et al., 2020) have shown an opposite trend compared to the finding in Figure 4. This might be due to the different setups and FBD dimensions used in their investigations, as they kept the number of particles (instead of the initial bed height) constant when the bed diameter was varied. The material to be dried, the particle size and the air velocity were also different.

For a fixed bed height, more SPW particles can be loaded into the FBD with a larger diameter, which means that there is more water content in those particles. More water needs to be evaporated to achieve the same dryness. Moreover, it is postulated that the wall contact surface area increases when the diameter of FBD increases, resulting in a more significant wall effect and therefore higher minimum fluidisation velocity is required. This is supported by the results in fluidised bed height. It is observed that the fluidised bed height is decreased by 56.7% with the increase of bed diameter from 140 mm to 210 mm. As the bed diameter increases, it is more difficult to fluidise the particle and thus the fluidised height decreases, leading to poorer drying performance. The current air velocity of 1.3 m/s is insufficient to provide effective fluidisation for better drying results. A higher minimum fluidisation velocity is necessary to fluidise more SPW particles presented in the FBD with a greater bed diameter.

Figure 4 Final moisture content ratio of SPW at v = 1.3 m/s and T = 50°C when bed height is kept at 220 mm (see online version for colours)

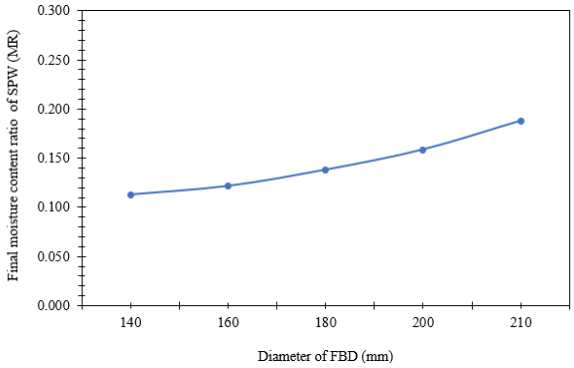

When the bed height is varied while the bed diameter is kept constant, the final moisture content ratio of the SPW particles is depicted in Figure 5. The trend in Figure 5 is the opposite of what is noticed in Figure 4. The reduction in the final moisture content ratio by 22.6% is reported when the FBD height is increased from 190 mm to 260 mm. The final moisture content ratio of SPW particles is at its minimum when the bed height is at its maximum. It is postulated that when the height of the FBD increases, the air region on top of the SPW particles increases. Hence, more air particles in the air region can take in the water evaporated from the SPW particles during the drying process, leading to a lower final moisture content ratio at a greater height of FBD.

Figure 5 Final moisture content ratio at v = 1.3 m/s and T = 50°C when bed diameter is kept at 180 mm (see online version for colours)

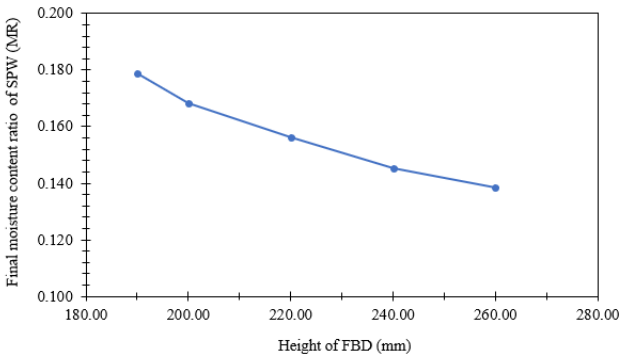

For the current boundary condition implemented, it is recommended to use a smaller bed diameter or higher FBD height for better drying performance. If a greater bed diameter is needed, higher air velocity and temperature are required for improved drying of the SPW particles. An air

temperature greater than 50°C can be employed for a greater driving force to evaporate water in the SPW particles to achieve a lower final moisture content ratio.

5.2 Effect of inlet air temperature on the drying of SPW

The inlet air temperature was differed in the values of 50°C, 70°C, and 100°C, and their influence on the drying of SPW was studied. Results attained in Figure 6 show that the final moisture content ratio of SPW is inversely proportional to the inlet air temperature. The final moisture content ratio of SPW decreases gradually to 0.151, 0.144, and 0.128 when the inlet air temperature increases from 50°C to 70°C, and then to 100°C, respectively. During the fluidisation process, the evaporation process is supposed to be taking place at the same time. As the supplied inlet air temperature increases, it increases the drying force for heat transfer, and hence, accelerates the drying process. Moreover, air with higher temperatures has lower relative humidity, hence, it has a greater capacity to capture water from the SPW particles. The moisture diffusivity is higher too. These results are consistent with the data of Suherman et al. (2018). Moreover, the volume fraction contour in Figure 7 shows that the volume fraction of SPW after drying is higher when the inlet temperature is 100°C if compared to the case of 50°C. Greater temperature can heat the fluidisation bed at a faster rate and hence the SPW is dried better, with a lower final moisture ratio. Since the final moisture ratio is lower, the volume fraction of SPW is higher.

Figure 6 Final moisture content ratio of SPW at v = 1.3 m/s in FBD with diameter of 180 mm and height of 220 mm (see online version for colours)

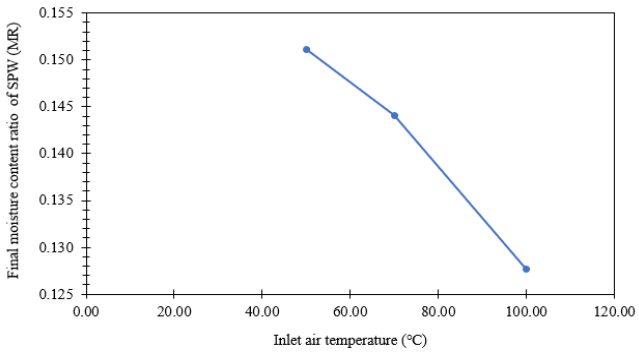

5.3 Effect of air velocity on the drying of SPW

Based on the results obtained in Figure 8, it is known that the final moisture contents of the SPW achieved at the end of the drying process in the FBD are gradually increasing with the increase of inlet air velocity. They are 0.154, 0.249, and 0.296 when the inlet air velocity is 1 m/s, 3 m/s, and 4 m/s, respectively. Rationally, when the inlet air velocity increases, the final moisture content is supposed to be decreased since there will be more collisions between the SPW particles and the air particles due to higher air velocity. In contrast, the results achieved are showing else wise. It is postulated that when the inlet air is entering the FBD at a greater velocity, more forceful collisions between the two phases occur, making some of the SPW particles forced to leave their initial bed height during the fluidisation process in FBD. This can be seen from the fluidisation contour in Figure 9. The SPW particles seem to fluidise vigorously at the increment of air velocity. Since the SPW particles are forced to leave the bed at a faster rate, there is no sufficient time for drying. If this is the case, higher inlet air temperature can be supplied for better drying. Some researchers also agree that it is not necessary to operate the FBD under high fluidisation velocity, the fluidised drying can retain high efficiencies even at low velocity (Dincer and Rosen, 2013). Rosli et al. (2018) claimed that an air velocity of 1 m/s to 2.2 m/s is sufficient for the fluidisation of SPW with a particle size of 2,000 m. Therefore, the air velocities of 3 m/s and 4 m/s considered in this study are too high, which results in the entrainment of SPW particles outside the bed, making the drying ineffective.

Figure 7 Volume fraction contour of SPW at v = 1.3 m/s in FBD with diameter of 180 mm and height of 220 mm for different inlet air temperatures (A) 50°C and (B) 100°C (see online version for colours)

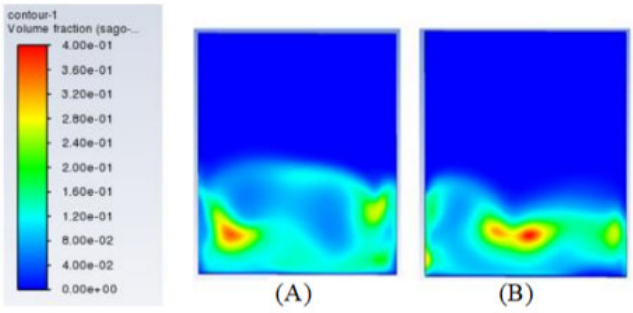

Figure 8 Final moisture content ratio of SPW at T = 50°C in FBD with diameter of 180 mm and height of 220 mm (see online version for colours)

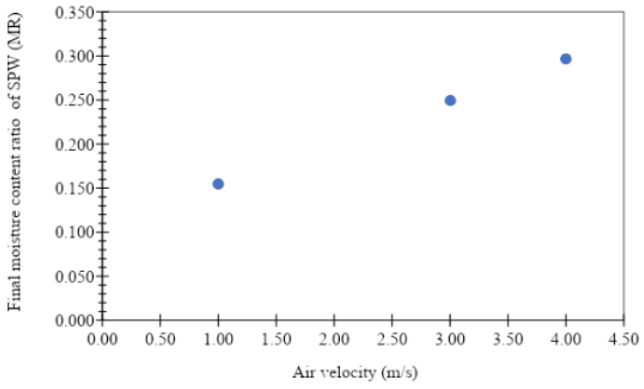

From Figure 9, the bed height of the SPW particles after fluidisation is more flattened when the inlet air velocity is 1 m/s. The bed height obtained has slightly increased to about 0.027 m compared to its original bed height of 0.023 m. When the inlet air velocity is 3 m/s, there is more vigorous fluidisation in the FBD and the SPW particles have left their

original bed height and fluidised across the FBD. According to the contour captured, a greater amount of them are around the walls and nearer to the outlet of the FBD. The air particles have forced the SPW particles to be pushed away from their initial position across the FBD. In like manner, the SPW particles are fluidising across the FBD when the inlet air velocity is 4 m/s. Some of the SPW particles might have overcome the pushing force caused by the air particles and returned nearer to the inlet area of the FBD. Hence, causing them to fluidise in a more even manner as noticed in the contour captured when the inlet air velocity is 4 m/s. Comparing the effect of air velocity and air inlet temperature on the final moisture content of SPW and the fluidised bed height, it can be concluded that air velocity has a more dominant role in determining the behaviour of the FBD.

Figure 9 Volume fraction contour of SPW at T = 50°C in FBD with diameter of 180 mm and height of 220 mm for different air velocities (A) 1 m/s, (B) 3 m/s, and (C) 4 m/s (see online version for colours)

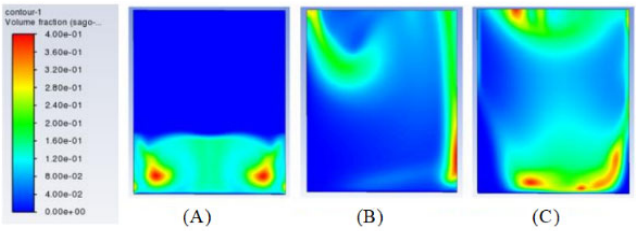

5.4 Summary

The desired final moisture content is 10%–20% to preserve the nutrients, and inhibit bacterial growth as well as for the common industrial packaging purposes for the conversion of SPW to animal feed or other value-added products (Othman et al., 2020; Rosli et al., 2018). With the initial moisture content of 40%, this corresponds to a desired final moisture content ratio of 0.25–0.50. From the results obtained, most of the cases studied in this research are having a final moisture content ratio smaller than 0.25. The recommended FBD diameter and height to achieve this desirable final moisture content range are 180 mm and 190 mm, respectively. Besides, to ensure the quality of the dried SPW, the drying time needs to be shortened so that the final moisture content is in the acceptable range. The optimal operating conditions are when the air velocities are in the range of 1–2 m/s and the inlet air temperature of 50°C.

6 Conclusions

The drying performance of SPW particles in an FBD with different dimensions was investigated numerically. Based on the results, it can be concluded that the dimensions of FBD, air inlet velocity, and air temperature play an essential role in determining the drying performance of SPW particles in the FBD. The findings of this study include:

1 More effective drying is achieved in the FBD with a smaller diameter but larger height.

2 The increment in air temperature can also enhance the drying of the SPW particles.

3 The air velocities of 3 m/s and 4 m/s are considered too high for the fluidisation of SPW particles with a size of 2,000 m. With these velocities, the SPW particles are noticed to entrain outside the bed height and thus leading to an ineffective drying performance.

4 Based on the setup of this present study, the recommended FBD dimension to achieve the desired final moisture content ratio of SPW of 0.25–0.50 is 180 mm diameter and 190 height. The optimal air velocities and air inlet temperature are 1–2 m/s and 50°C, respectively.

For future studies, it is recommended to measure the thermo-physical properties of SPW particles experimentally as the inputs for simulations. A more comprehensive 3D model can be employed for future investigation. The energy and exergy aspects of the SPW drying in the FBD can also be scrutinised.

References

Alaathar, I., Hartge, E-U., Heinrich, S. and Werther, J. (2013) 'Modeling and flowsheet simulation of continuous fluidized bed dryers', *Powder Technology*, Vol. 238, pp.132–141.

Amin, N.M., Sabli, N., Izhar, S. and Yoshida, H. (2019) 'A review: sago wastes and its applications', *Pertanika Journal of Science and Technology*, Vol. 27, No. 4, pp.1841–1862.

Ansys (2013) *ANSYS Fluent Theory Guide 15.0*, ANSYS, Inc., USA.

Awg-Adeni, D., Abd-Aziz, S., Bujang, K. and Hassan, M. (2009) 'Bioconversion of sago residue into value added products', *African Journal of Biotechnology*, Vol. 9, No. 14, pp.2016–2021.

Aziz, H., Ahsan, S.N., De Simone, G., Gao, Y. and Chaudhuri, B. (2022) 'Computational modeling of drying of pharmaceutical wet granules in a fluidized bed dryer using coupled CFD-DEM approach', *AAPS PharmSciTech*, Vol. 23, No. 1, p.59.

Azmir, J., Hou, Q. and Yu, A. (2018) 'Discrete particle simulation of food grain drying in a fluidised bed', *Powder Technology*, Vol. 323, pp.238–249.

Basrawi, M.F., Redzlan, F., Ibrahim, T.K. and Yudin, A.S.M. (2020) 'Experimental study on the effect of bed aspect ratio to the drying rate of chilli for swirling fluidized bed dryer', *IOP Conference Series: Materials Science and Engineering*, Vol. 863, p.12044.

Dincer, I. and Rosen, M.A. (2013) 'Chapter 10 – exergy analysis of drying processes and systems', in Dincer, I. and Rosen, M.A. (Eds.): *Exergy*, 2nd ed., Elsevier, Amsterdam.

Ehara, H., Toyoda, Y. and Johnson, D.V. (2018) *Sago Palm: Multiple Contributions to Food Security and Sustainable Livelihoods,* Springer Nature, USA.

Lai, J.C., Rahman, W.A.W. A. and Toh, W.Y. (2013) 'Characterisation of sago pith waste and its composites', *Industrial Crops and Products*, Vol. 45, pp.319–326.

Lamidi, R.O., Jiang, L., Pathare, P.B., Wang, Y.D. and Roskilly, A.P. (2019) 'Recent advances in sustainable drying of agricultural produce: a review', *Applied Energy*, Vols. 233–234, pp.367–385.

Li, W., Shen, K., Wei, D. and Wang, K. (2022) 'Simulation of heat transfer performance of silicone-based insulation coatings', *International Journal of Simulation and Process Modelling*, Vol. 18, No. 3, pp.211–221.

Liu, G. (2022) 'Experimental research and simulation verification of recycling process of heat transfer oil', *International Journal of Simulation and Process Modelling*, Vol. 18, No. 1, pp.45–60.

Mortier, S.T.F.C., De Beer, T., Gernaey, K.V., Remon, J.P., Vervaet, C. and Nopens, I. (2011) 'Mechanistic modelling of fluidized bed drying processes of wet porous granules: a review', *European Journal of Pharmaceutics and Biopharmaceutics*, Vol. 79, No. 2, pp.205–225.

Nabizadeh, A., Hassanzadeh, H., Asadieraghi, M., Hassanpour, A., Moradi, D., Keshavarz Moraveji, M. and Hozhabri Namin, M. (2020) 'A parametric study of the drying process of polypropylene particles in a pilot-scale fluidized bed dryer using computational fluid dynamics', *Chemical Engineering Research and Design*, Vol. 156, pp.13–22.

Nasir, A.M.I.A., Rosli, M.I., Takriffa, M.S., Othman, N.T.A. and Ravichandar, V. (2021) 'Computational fluid dynamics simulation of fluidized bed dryer for sago pith waste drying process', *Jurnal Kejuruteraan*, Vol. 33, No. 2, pp.239–248.

Othman, T.N.A., Din, Z.A.M. and Takriff, S. (2020) 'Simulation on drying of sago bagasse in a fluidized bed dryer', *Journal of Engineering Science and Technology*, Vol. 15, No. 4, pp.2507–2521.

Phang, S.M., Miah, M.S., Yeoh, B.G. and Hashim, M.A. (2000) 'Spirulina cultivation in digested sago starch factory wastewater', *Journal of Applied Phycology*, Vol. 12, pp.395–400.

Rao, A., Curtis, J.S., Hancock, B.C. and Wassgren, C. (2010) 'The effect of column diameter and bed height on minimum fluidization velocity', *AIChE Journal*, Vol. 56, No. 9, pp.2304–2311.

Rosli, M.I., Abdul Nasir, A.M.I., Takriff, M.S. and Chern, L.P. (2018) 'Simulation of a fluidized bed dryer for the drying of sago waste', *Energies*, Vol. 11, No. 9, p.2383.

Rosli, M.I., Abdul Nasir, A.M.I., Takriff, M.S. and Ravichandar, V. (2020) 'Drying sago pith waste in a fluidized bed dryer', *Food and Bioproducts Processing*, Vol. 123, pp.335–344.

Sarker, R., Rahman, M., Love, N. and Choudhuri, A. (2012) 'Effect of bed height, bed diameter and particle shape on minimum fluidization in a gas-solid fluidized bed', *50th AIAA Aerospace Sciences Meeting Including the New Horizons Forum and Aerospace Exposition*.

Singhal, R.S., Kennedy, J.F., Gopalakrishnan, S.M., Kaczmarek, A., Knill, C.J. and Akmar, P.F. (2008) 'Industrial production, processing, and utilization of sago palm-derived products', *Carbohydrate Polymers*, Vol. 72, No. 1, pp.1–20.

Suherman, S., Azaria, N.F. and Karami, S. (2018) 'Performance study of fluidized bed dryer with immersed heater for paddy drying', *IOP Conference Series: Materials Science and Engineering*, Vol. 316, p.12026.

Tayyeb, N., Arezou, J., Mohammad Hossein, K. and Mortaza, A. (2013) 'CFD simulation and optimization of factors affecting the performance of a fluidized bed dryer', *Iranian Journal of Chemistry and Chemical Engineering*, Vol. 32, No. 4, pp.81–92.

Zhu, F. (2019) 'Recent advances in modifications and applications of sago starch', *Food Hydrocolloids*, Vol. 96, pp.412–423.